

PACS numbers: 52.50.Jm; 52.38.Ph
DOI: 10.1070/QE2004v034n07ABEH002647

Measurements of the xenon density in a pulsed jet from absorption of monochromatic soft X-rays

A.S. Boldarev, V.A. Gasilov, V.E. Levashov, K.N. Mednikov,
A.S. Pirozhkov, M.S. Pirozhkova, E.N. Ragozin

***Abstract*. The density distribution in a pulsed xenon gas jet emanating through cylindrical and conic (supersonic) nozzles in vacuum was investigated experimentally and theoretically for different stagnation pressures and at different instants of time. The measurements were made from absorption of monochromatic soft X-rays (SXRs) ($\lambda = 13.6$ nm) produced by a nanosecond laser-plasma source. Focusing normal-incidence multilayer mirrors were employed for the monochromatisation of soft X-rays and the production of transmission jet images (X-ray absorption patterns). Numerical simulations were made of the transient outflow of xenon in vacuum taking cluster production into account. The measured absolute density values and the density distribution agree nicely with the simulations.**

Keywords: *pulsed xenon jet, laser plasma, soft X-rays, xenon clusters, multilayer mirrors.*

1. Introduction

As is generally known, the use of nanosecond soft X-ray (SXR) pulses enables investigations of transient objects and phenomena to be made from absorption of radiation at different instants of time. One such object of considerable practical interest is a pulsed gas jet in vacuum. In particular, a partially clusterised xenon jet is considered as the laser target for a 'clean' (debris-free) laser-plasma SXR source for the projection X-ray microlithography, absorption spectroscopy, reflectometry etc., which exerts scarcely any adverse effect on the surrounding optics (see, for instance, Refs [1 – 3]). The interaction of high-power laser radiation with clusters is of considerable interest as a source of specific high-temperature plasmas, high-energy particles and photons, etc. [4 – 6]. While on the subject of other applications of a pulsed gas jet, mention should be made of the relatively long-pursued investigations aimed at the development of SXR – VUV lasers utilising the transitions of Ne-, Ni-, and Pd-like ions excited by laser radiation [7, 8] as well as of the generation of high-order harmonics of laser radiation whose spectrum extends into the SXR region to ~ 10 nm and below [9, 10]. Recently, a start was made on the experiments on the spectroscopic observation of the charge exchange of multiply charged laser-plasma ions with the donor atoms in a rare-gas jet [11, 12]. In this connection effort was recently mounted to experimentally characterise and theoretically simulate a rare-gas pulsed jet (including a supersonic jet) in vacuum (see, for instance, Refs [13 – 15]). In this case, the density measurements of a xenon jet were carried out by the interferometric technique.

In this work, we carried out an experimental and theoretical investigation of the density distribution in a pulsed xenon gas jet emanating through cylindrical and conic (supersonic) nozzles in vacuum. We have developed a technique for measuring the density distribution in the jet from its transmission images obtained by backlighting it with a SXR pulse. These images (X-ray absorption patterns) are formed with the aid of focusing multilayer optics, which simultaneously fulfils the function of radiation monochromatisation. In this case, the information on the jet density resides in the intensity attenuation factor for the rays transmitted through different regions of the jet. The measurements were carried out for different pressures in the stagnation chamber* and at different points in time after the onset of gas nozzle flow. The gas dynamic flow was numerically simulated in the context of the model of Ref. [16] with the inclusion of cluster production, which accompanies the fast cooling of gas in its expansion in vacuum. The density was determined from the X-ray absorption patterns of the jet in two ways. The first relied on the form of the radial density distribution $N_{\rm th}(r, z_0)$ at a section z_0 derived by the numerical simulations, and a density value $fN_{\rm th}(r, z_0)$ was selected whereby the calculated absorption showed the best fit to the X-ray absorption patterns (for brevity, hereafter this technique will be referred to as the direct fit). In the second approach, the radial density distribution was determined using the Abelian transformation. The use of monochromatic radiation furnished a rather high accuracy of absolute density measurements ($\sim 10\,\%$), while the selection of a wavelength close to the peak of the xenon absorption band ensured a high (in comparison with the interferometry of the visible range) sensitivity of our technique.

A.S. Boldarev, V.A. Gasilov Institute of Mathematical Modeling, Russian Academy of Sciences, Miusskaya pl. 4a, 125047 Moscow, Russia;
V.E. Levashov, K.N. Mednikov, A.S. Pirozhkov, M.S. Pirozhkova, E.N. Ragozin P.N. Lebedev Physics Institute, Russian Academy of Sciences, Leninskii prosp. 53, 119991 Moscow, Russia;
e-mail: enragozin@sci.lebedev.ru

Received 11 March 2004
Kvantovaya Elektronika **34** (7) 679 – 684 (2004)
Translated by E.N. Ragozin

*By the stagnation pressure is meant the pressure of immobile gas prior to the opening of a pulsed valve.

2. Experiment

Determination of the gas jet density profile involves comparison of the intensities of the probe monochromatic SXRs transmitted through different regions of the jet (Fig. 1):

$$I(y,\lambda_0) = I_0(\lambda_0)\exp[-\tau(y,\lambda_0)],$$

where $I_0(\lambda_0)$ is the initial intensity of the probe monochromatic radiation with a wavelength λ_0;

$$\tau(y,\lambda_0) = 2\sigma_a\int_0^\infty N(r=(x^2+y^2)^{1/2})\mathrm{d}x$$

is the optical thickness along the ray passing parallel to the x axis at a distance y from the jet axis (the jet is assumed to be axially symmetric); N is the atomic number density; $\sigma_a = 2r_e\lambda_0 f_2$ is the absorption cross section (per atom); r_e is the classical electron radius; and f_2 is the imaginary part of the atomic scattering factor. The refraction in the jet was insignificant and was therefore neglected (see below). The SXR absorption at a given wavelength is independent of the aggregate state of a substance (in this case, on the degree of xenon clusterisation) and depends only on the integral density along the ray trajectory $[2\int_0^\infty N(r)\mathrm{d}x]$ and the atomic number of the element (i.e., on f_2). The data on the atomic scattering factors are available from the literature for elements with nuclear charges from 1 to 92 in the 30-eV–30-keV photon energy range [17, 18].

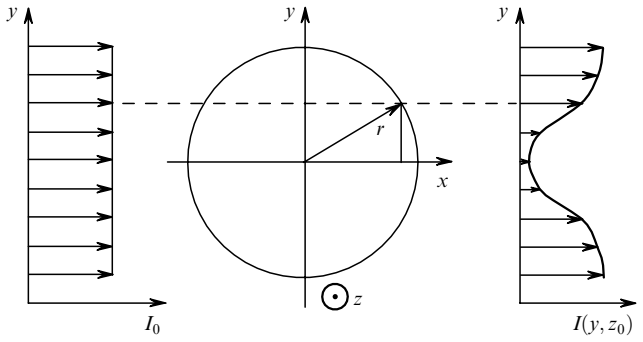

Figure 1. Scheme explaining the technique of density measurements from the absorption of monochromatic radiation.

The gas jet was backlighted by SXR pulses from the plasma produced by irradiating a tungsten target with the focused pulses of a solid-state laser utilising neodymium-doped yttrium ortho-aluminate crystals ($Nd:YAlO_3$, $\lambda = 1.08$ μm, $Q = 0.4$ J, $t = 6$ ns). The experimental setup for recording the X-ray absorption patterns of the pulsed jet is represented schematically in Fig. 2. In the majority of experiments, laser plasma (*1*) was located at a distance of 62 mm from the jet axis. The gas jet in vacuum was produced with high pressure pulsed electromagnetic valve (*2*) timed with the laser shot. The gas pressure in the stagnation region was varied; its upper limit was equal to 10 atm. The jet axis lies in the plane of the draft. Similar multilayer mirrors (MMs) (*4*) and (*5*) (with diameters of 40 mm and a 1-m radius of curvature, $\lambda_0 = 13.6$ nm) imaged the plane containing the nozzle axis onto UF-4 X-ray photographic film (*7*) shielded from the visible and UV light by absorption filter (*6*) fabricated in the Institute for the Physics of Microstructures, Russian Academy of Sciences [19]. Filter (*6*) was a mesh-supported Nb/Si multilayer structure with a net transmittance of 41 % at a wavelength of 13.5 nm. The filter was located at a distance of 60 mm from the photographic film, at about the same place as the source image, which measured ~ 100 μm. This allowed us to obviate the illumination nonuniformity of the field of view arising from the filter-supporting mesh with a period of 0.5 mm. The combination of two MMs and the absorption filter fulfilled the functions of monochromatisation of the recorded radiation and reliable background suppression.

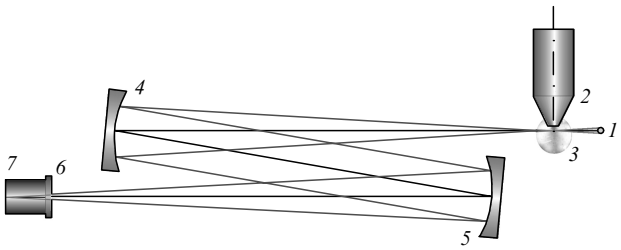

Figure 2. Scheme of the experimental setup for recording X-ray absorption patterns of a pulsed gas jet: (*1*) plasma of a tungsten laser target; (*2*) high-pressure pulsed gas valve; (*3*) field of view of the optical system of two multilayer mirrors (*4*) and (*5*) (1-m radius of curvature, $\lambda_0 = 13.6$ nm); (*7*) UF-4 X-ray photographic film shielded from the visible and UV light by an absorption filter (*6*).

The selection of the 13.6-nm probe radiation wavelength is explained by the fact that it is within a strong Xe absorption band (Fig. 3), which furnishes a rather high sensitivity of the technique. If an optical thickness $\tau(y = 0, \lambda_0) = 0.25$ is conventionally adopted as the threshold of recording, the threshold column density of xenon is equal to 10^{16} atom cm^{-2}. This threshold column density is approximately 20 times lower than in interferometric measurements.

X-ray absorption patterns were recorded in one laser shot, a laser beam with an energy below 0.4 J being used to avoid overexposure of the X-ray photographic film. Exemplified in Fig. 4 are X-ray absorption patterns of the xenon jet obtained in the gas flow through cylindrical and conic nozzles at different stagnation pressures. The cylindrical

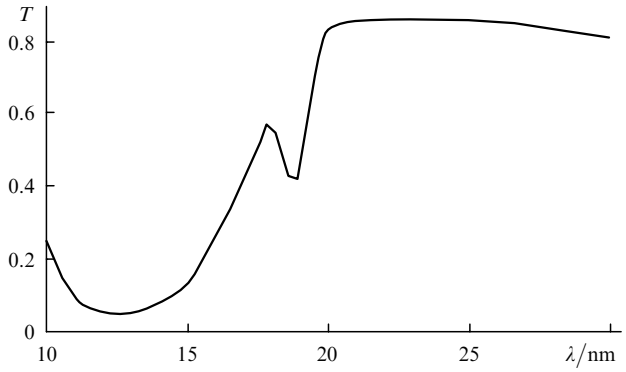

Figure 3. Transmittance of a xenon layer with a column density of 1.1×10^{17} atom cm^{-2}.

nozzle was a channel 0.4 mm in diameter, while the conic nozzle had an outlet 1 mm in diameter for an outlet–inlet area ratio $S_{out}/S_{in} \approx 5$. Assuming xenon to be an ideal gas and the gas flow to be uniform over the nozzle cross section, the Mach number M at the nozzle outlet can be estimated by the formula $S_{out}/S_{in} \approx \frac{9}{16} M^{-1}(1 + M^2/3)^2$ [20], hence we obtain $M \approx 3.8$. Numerical simulations taking into account the specific geometry of the nozzle yields $M = 4.2 - 4.35$ and a flow velocity of 2.8×10^4 cm s^{-1}. As would be expected, the X-ray absorption patterns of the jet are qualitatively different for cylindrical and conic nozzles. This accounts for the difference in the nature of hydrodynamic flows: for a conic nozzle, the lateral jet expansion is significantly smaller (the jet as if lives longer). Of course, the density at the nozzle outlet is lower in this case than for a cylindrical nozzle and the same stagnation gas pressure. This is illustrated in Fig. 5, which depicts the density distributions $N_{th}(r, z_0)$ at three sections ($z_0 = 0.5$, 1.0, and 1.5 mm) in the outflow of xenon through the conic and cylindrical nozzles for the same stagnation pressure (3.76 atm). One can see that the axial jet density in the supersonic outflow remains almost invariable up to a distance of one and a half millimetres from the nozzle orifice.

Emphasis should be placed on the 'spectral purity' of radiation in the experimental determination of gas density. Let the radiation incident on the detector contain, along with the radiation with the λ_0 wavelength, the background radiation with an intensity I_b whose wavelength range is beyond the xenon absorption band. Then, the apparent optical thickness for a ray passing through the jet axis is

$$\tau_{app}(y = 0, \lambda_0) = \ln \frac{1 + I_b/I_0(\lambda_0)}{\exp[-\tau(y = 0, \lambda_0)] + I_b/I_0(\lambda_0)}. \quad (1)$$

For simplicity we assume that $\tau(y = 0, \lambda_0) = 4$ – this value enables the radial density distribution to be measured at distances to the jet axis equal to several characteristic radii. Let us assume that the relative background intensity amounts to 1 % [$I_b/I_0(\lambda_0) = 0.01$]. Then, the apparent optical thickness for the ray passing through the jet axis is $\tau_{app}(y = 0, \lambda_0) = 3.57$, which signifies underestimating the density by 11 %. A relative background intensity of 10 % entails an almost twofold error in the density measurement.

In our experiment it was possible to afford a sufficiently high 'spectral purity' of the radiation recorded. Figure 6 shows the wavelength dependences of the reflectivities of one [curve (*1*)] MM and two [curve (*2*)] sequentially placed MMs. Our attention is engaged by a relatively weak (in comparison with the resonance reflection peak) wing extending over tens of nanometres to the long-wavelength side. For a spectrally uniform source intensity distribution this wing may be responsible for a departure of the measured (apparent) xenon density from the true one. Figure 7 depicts the calculated apparent optical thickness τ_{app} as a function of the real optical thickness τ for one-mirror [MM + filter, curve (*1*)] and two-mirror [MM + MM + filter, curve (*2*)] configurations with a broadband radiation source. In the hypothetical case of monochromatic light, $\tau_{app} \equiv \tau$ [straight line (*3*)]. One can see from Fig. 7 that the one-mirror setup would introduce an appreciable (20 %) error even for $\tau \sim 5$. In reality, the departure of curves (*1*) and (*2*) from the straight line (*3*) may be somewhat larger owing to the filter transparency window in the 40–50 nm range neglected in the calculation. The dynamic range of the X-ray photographic film allows comparing the intensities which diverge by approximately two orders of magnitude (this corresponds to $\tau \sim 5$), while the employment of AXUV X-ray photodiodes, whose linearity range amounts to eight orders of magnitude, makes it basically possible to carry out measurements up to $\tau \sim 15$.

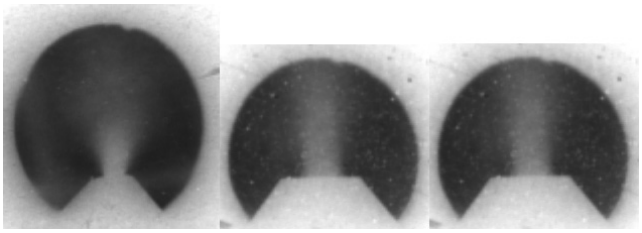

a b c

Figure 4. Examples of the X-ray absorption patterns of a xenon jet obtained when the gas flowed through cylindrical (a) and conic (b, c) nozzles. The stagnation pressure was 1 (a, b) and 3.7 atm (c).

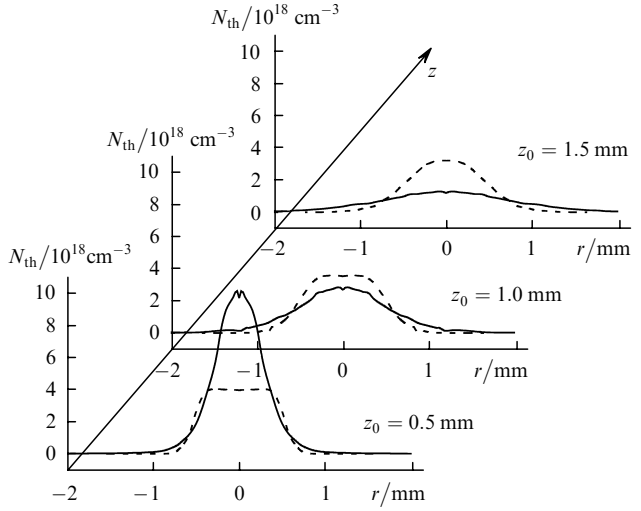

Figure 5. Simulated density distributions $N_{th}(r, z_0)$ at three sections ($z_0 = 0.5$, 1.0, and 1.5 mm) in the outflow of xenon through the conic (dashed curves) and cylindrical (solid curves) nozzles for the same stagnation pressure (3.76 atm).

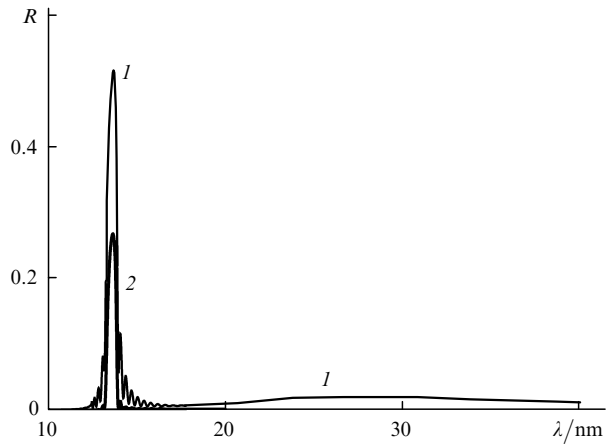

Figure 6. Reflectivities of one (*1*) MM and two (*2*) sequentially arranged MMs.

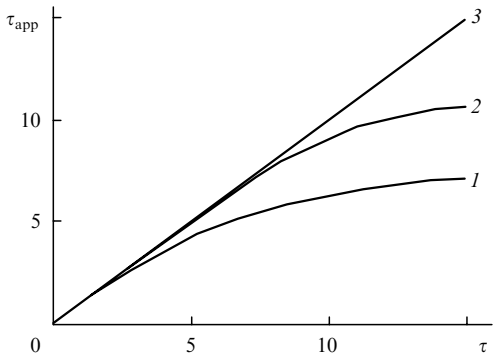

Figure 7. Apparent (i.e. experimentally measured) optical thickness τ_{app} as a function of real optical thickness τ for the one-mirror [MM + filter, (*1*)] and two-mirror [MM + MM + filter, (*2*)] setups with a broadband radiation source. The straight line $\tau_{app} = \tau$ (*3*) corresponds to the case of ideal monochromatisation.

3. Processing of X-ray absorption patterns and measurement data

The Abelian transformation furnishes a mathematically rigorous solution of the problem of reconstruction of an axially symmetric density distribution from absorption images. However, in the practical application of this method there quite often arose solutions oscillatory about the axis and therefore unacceptable from the physical standpoint. The reason lies with a constant component of noise at the periphery of the image, whence the density profile reconstruction makes a start. It is pertinent to note that numerical hydrodynamic simulations also yield a nonmonotonic run of the $N_{th}(r)$ curve. So, to reconstruct the profile requires a large signal–noise ratio at the periphery of the image. With trustworthy simulations, we can restrict ourselves to determination of only one adjustable parameter in the direct fit technique. In our work, use was made for the most part of precisely this technique.

The hydrodynamic simulations of the transient outflow of gas through cylindrical and conic nozzles in vacuum were carried out for different pressures in the gas stagnation range. They showed that the fraction of clusterised substance is small under our experimental conditions (room temperature, moderate gas pressure): for a pressure of ~ 3.8 atm and a conic nozzle, for instance, the fraction of clusterised xenon atoms is equal to $\sim 10^{-4}$. Because of this, the gas density field $N_{th}(r, z)$ is virtually proportional to the stagnation pressure. We are concerned with the xenon parameters at distances $z_0 = 0 - 1.5$ mm to the nozzle orifice. The purely hydrodynamic settling time for the flow within this range is shorter than 100 μs, while the time interval between the onset of plunger motion and the instant of maximum valve transmission is equal to 80 μs. On this basis we believe that the actual flow settling time does not exceed ~ 100 μs, either.

A comparison of experimental and calculated intensity profiles revealed that the experimental profile was somewhat broader. This made us into the assumption that there existed instrumental scattering, which was borne out by the presence of blackening background in the region of geometrical shadow in X-ray absorption patterns. The scattering took place in the reflection of the radiation from the MMs and in its passage through the absorption filter. Additional experiments with a different arrangement of the filter and the mirrors which might reveal the relative contribution of these elements to the total scattering were not conducted. When taking the scattering into account we assumed that its intensity distribution profile was Gaussian and the fraction of scattered component energy was equal to 1/3 of the total energy. This corresponds to the scattering from a mirror with a one-metre radius, a surface roughness $\sigma = 0.7$ nm, and a correlation radius of surface irregularities $a = 5$ μm. On inclusion of scattering in the X-ray optical system with these parameters, which are typical for MM substrates, the form of the calculated intensity profile $I_{th}(r, z)$ corresponded almost perfectly with the experimental profile $I(r, z)$. In doing so the absolute density values changed by about 10 %.

It was assumed that the xenon jet was optically uniform and did not scatter the 13.6-nm probe radiation. We briefly substantiate this assumption. Two effects may be involved. First, the radiation may experience refraction owing to the density gradient in the Xe jet. This may be of importance when the angle of refraction is comparable to the acceptance angle of the X-ray optical system, so that part of the radiation does not arrive at the detector and fails to participate in the jet image formation. In our case, the angular acceptance is equal to 0.08 rad. The maximum angle of refraction in transit through the jet is $\sim |n - 1| = \delta$, where δ is the real addition to the index of refraction $\sim |n - 1| = \delta$. The maximum addition within the reflection band of the MMs is $\delta = 1.1 \times 10^{-5}$ (for a Xe atomic number density of 10^{19} cm^{-3}), and therefore refraction is insignificant in the context of our experiment.

Second, the scattering from clusters may take place. The fraction of radiation interacting with clusters amounts to $\sim \pi r_{cl}^2 N_{cl} d_{0.5}$, where $r_{cl} \approx 0.05$ is the average radius of xenon clusters (the conic nozzle, a stagnation pressure of 3.76 atm); $N_{cl} \approx 3 \times 10^7$ cm^{-3} is the cluster number density on the jet axis; and $d_{0.5} \approx 1$ mm is the jet diameter. Hence it is evident that $\pi r_{cl}^2 N_{cl} d_{0.5} \approx 2.4 \times 10^{-4} \ll 1$, so that the scattering from the clusters can also be neglected.

In the processing of X-ray absorption patterns by the direct fit technique, use was made of the radial density distribution borrowed from the simulations, which was multiplied by an adjustable coefficient, $f N_{th}(r, z_0)$. Then, the adjustable coefficient f was selected from the best fit of the calculated and experimental intensity profiles at three sections: $z_0 = 0.5$, 1.0, and 1.5 mm.

Fig. 8a shows the experimental radial intensity profile $I(r, z_0 = 0.5$ mm) at the section perpendicular to the jet axis at a distance of 0.5 mm to the nozzle orifice as well as its approximation by the calculated intensity profile at this section. The latter relies on the hydrodynamic simulation of the density profile $N_{th}(r, z_0 = 0.5$ mm) (Fig. 8b) and the inclusion of scattering. The best fit is obtained for $f \approx 0.73$. A similar approximation at the sections $z_0 = 1.0$ and 1.5 mm yielded $f \approx 0.77$ and 0.75, respectively. As noted above, the inclusion of scattering results in only a ~ 10 % change of the absolute value of axial density but enables gaining a better agreement between the shapes of the calculated and experimental intensity profiles. A similar ratio between the experimental and simulated density profiles was obtained in the outflow of xenon through the cylindrical nozzle and a stagnation pressure of 1 atm: the experimental density values at three sections ($z_0 = 0.5$, 1.0, and 1.5 mm) were equal to about 3/4 of the simulated ones.

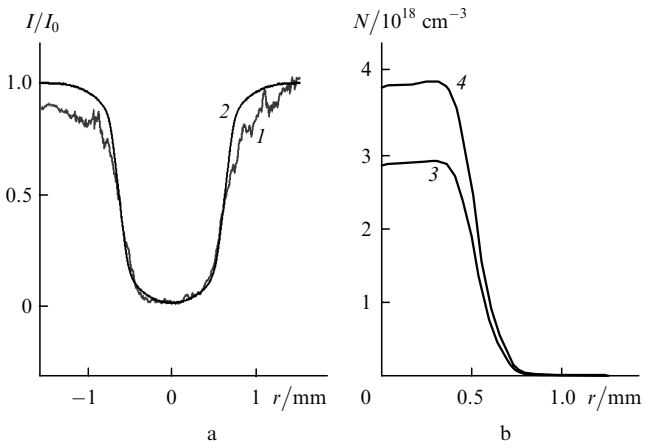

Figure 8. Experimental radial intensity profile $I(r, z_0 = 0.5$ mm) at the section perpendicular to the jet axis passing at a distance of 0.5 mm to the nozzle orifice (*1*) and its approximation by the calculated intensity profile at this section (*2*) (a) as well as experimental (*3*) and simulated (*4*) density profiles (b). The density profile (*3*) corresponds to the experimental intensity profile (*1*).

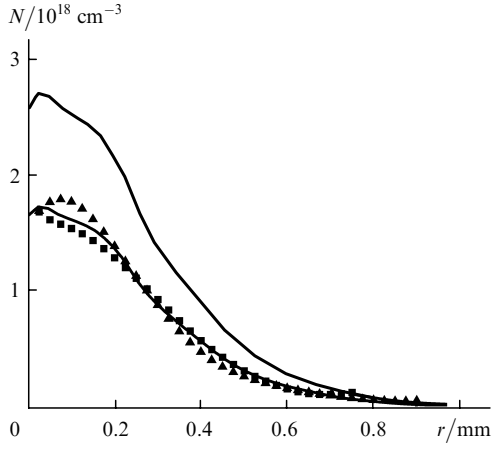

Figure 9. Radial density profile $N_A(r, z_0 = 0.5$ mm) (points), reconstructed employing the Abelian transformation from two parts of the X-ray absorption pattern lying on the opposite sides of the image axis (the cylindrical nozzle, a xenon stagnation pressure of 1 atm). The upper curve (N_{th}) is the numerical simulation, the lower curve (fN_{th}) represents the theoretical values multiplied by the factor $f = 0.64$.

We also determined the radial density distribution with the aid of the Abelian transformation [21] in the cases when the noise of X-ray photographic film allowed this to be performed. In Fig. 9, the profile $N_A(r, z_0 = 0.5$ mm) reconstructed employing the Abelian transformation (the cylindrical nozzle, a xenon stagnation pressure of 1 atm) is compared with the $N_{th}(r, z_0 = 0.5$ mm) profile obtained by way of hydrodynamic simulation (the upper curve). The lower curve is the same theoretical profile multiplied by a factor of 0.64. This comparison shows that the hydrodynamic simulations provide an adequate description of the radial density profile. However, the absolute density values derived by the direct fit technique corresponded to a somewhat higher value of the adjustable coefficient: $f \approx 0.75$ (see above).

As indicated earlier, the dynamic range of the X-ray photographic film is relatively narrow and does not allow a comparison of intensities that differ by more than a factor of 100. (This corresponds to an optical thickness $\tau \sim 5$). In spite of this circumstance, we managed to process X-ray absorption patterns of the jet at sections wherein the maximum optical thickness amounted to about 20. Although the central (paraxial) region of the image is no longer sensitive to the gas density in this case, this region expands in the radial direction with increasing density. This makes it possible to select the coefficient f with a reasonably high precision by employing the direct fit technique and fitting the calculated intensity profile to the calculated one. In particular, for a stagnation pressure of 3.66 atm and a xenon outflow through the cylindrical nozzle we obtained: $N(r = 0, z_0 = 0.5$ mm$) = (1.06 \pm 0.1) \times 10^{19}$ cm^{-3}, or about 1.1 ± 0.1 of the simulated density ($\tau \approx 17$); $N(r = 0, z_0 = 1.0) = (2.4 \pm 0.25) \times 10^{18}$ cm^{-3}, or about 0.88 ± 0.1 of the simulated density ($\tau \approx 8$).

The theoretical (hydrodynamic simulations) and experimental (direct fit) axial density values at three sections ($z_0 = 0.5$, 1.0, and 1.5 mm) for different stagnation pressures and both nozzle types are collected in Table 1; for convenience, the adjustable coefficient f is indicated in parentheses. From the tabulated date one can draw a conclusion that the discrepancy between the theory and the experiment somewhat decreases with increasing stagnation pressure. This may be attributed to the fact that to higher stagnation pressures there correspond larger optical thicknesses and larger image dimensions, and the noise of the X-ray photographic film diminishes in importance. Furthermore, the discordance between the simulated and experimental density may be due to the fact that the real conditions for the gas flow into the nozzle are different from the ideal ones prescribed in the simulations. In experiment, in particular, the stagnation chamber contains partitions with openings and a moving rod, which is hard to faithfully reproduce in numerical simulations. Some uncertainty may arise from the inexact knowledge of the run of the characteristic curve of the X-ray photographic film, of the atomic scattering factors, etc. To summarise our analysis, it may be safely suggested that the absolute density values in the xenon jet fall within the range between 0.75 and 1.0 of the simulated density in the gas outflow both through the cylindrical and conic nozzles.

Table 1. On-axis xenon density (in cm^{-3}).

Type of nozzle	Pressure/atm	$z_0 = 0.5$ mm		$z_0 = 1$ mm		$z_0 = 1.5$ mm	
		Theory	Experiment	Theory	Experiment	Theory	Experiment
Cone	3.76	4×10^{18}	2.9×10^{18} ($f = 0.73$)	3.55×10^{18}	2.73×10^{18} ($f = 0.77$)	3.2×10^{18}	2.4×10^{18} ($f = 0.75$)
Cone	3.36	3.57×10^{18}	2.8×10^{18} ($f = 0.78$)	3.17×10^{18}	2.56×10^{18} ($f = 0.8$)	2.87×10^{18}	2.1×10^{18} ($f = 0.73$)
Cone	1	1.03×10^{18}	6.2×10^{17} ($f = 0.6$)	9.2×10^{17}	5.5×10^{17} ($f = 0.6$)	8.3×10^{17}	4.7×10^{17} ($f = 0.57$)
Cylinder	1	2.65×10^{18}	2.0×10^{18} ($f = 0.77$)	7.4×10^{17}	5.75×10^{17} ($f = 0.78$)	3.3×10^{17}	2.5×10^{17} ($f = 0.76$)
Cylinder	3.66	9.7×10^{18}	1.06×10^{19} ($f = 1.1$)	2.7×10^{18}	2.4×10^{18} ($f = 0.88$)	–	–

4. Conclusions

We have elaborated a technique for measuring the density of a pulsed gas jet from the absorption of monochromatic radiation in the SXR spectral region. The SXR pulse was produced by irradiating a tungsten target by the focused beam of an Nd : $YAlO_3$ laser ($\lambda = 1.08$ μm, $Q = 0.4$ J, $t =$ 6 ns). The X-ray absorption patterns of the pulsed xenon jet were constructed with the aid of focusing normal-incidence MMs combined with a multilayer absorption filter. For xenon, the sensitivity (the threshold column density) of the technique is about 10^{16} atom cm^{-2} at a wavelength of 13.6 nm. Gas-dynamic simulations were made of the pulsed xenon jet flowing out through cylindrical and conic nozzles in vacuum. X-ray absorption patterns were recorded at the stage of stationary jet flow for both nozzles for different xenon pressures in the stagnation chamber. The processing of the X-ray absorption patterns revealed that the radial density distribution at different distances to the nozzle corresponds to the simulated distributions, while the absolute density values lie in the range from 0.75 to 1.0 of the values obtained in the simulations.

Acknowledgements. The authors thank N.N. Salashchenko and V.I. Luchin for placing at our disposal multilayer absorption filters and E.Ya. Kononov and A.N. Ryabtsev for their cooperation in the processing of X-ray absorption patterns. This work was supported by the Russian Foundation for Basic Research (Grant Nos 04-02-16209, 02-01-00708); the 'Optical Spectroscopy and Frequency Standards' Basic Research Programme of the Physical Sciences Division, Russian Academy of Sciences; and the BRHE (CRDF) 2003 Programme (Y1-P-11-04, REC-011).

References

1. De Bruijn R., Bartnik A., Fiedderus H.F., Fiedorowicz H., Hegeman P., Constantinescu R.C., Bijkerk F. *Proc. SPIE Int. Soc. Opt. Eng.*, **3997**, 157 (2000).
2. Suzuki M., Daido H., Choi I.W., Yu W., Nagai K., Norimatsu T., Mima K., Fiedorowicz H. *Phys. Plasmas*, **10** (1), 227 (2003).
3. Stiel H., Vogt U., Ter-Avetysian S., Schnürer M., Will I., Nickles P.V. *Proc. SPIE Int. Soc. Opt. Eng.*, **4781**, 26 (2002).
4. Lezius M., Dobosz S., Normand D., Schmidt M. *Phys. Rev. Lett.*, **80** (2), 261 (1998).
5. Ditmire T., Gumbrell E.T., Smith R.A., Djaoui A., Hutchinson M.H.R. *Phys. Rev. Lett.*, **80** (4), 720 (1998).
6. Ditmire T., Donnelly T., Falcone R.W., Perry M.D. *Phys. Rev. Lett.*, **75** (17), 3122 (1995).
7. Fiedorowicz H., Bartnik A., Kostecki J., Szczurek M., Fill E., Li Y., Lu P., Pretzler G., Nilsen J. *Proc. V Int. Conf. on X-Ray Lasers* (Lund, Sweden, 1996; Bristol: IOPP, 1996) p. 76.
8. Lu P., Kawachi T., Suzuki M., Sukegawa K., Namba S., Tanaka M., Hasegawa N., Tai R., Kishimoto M., Kado M., Nagashima K., Daido H., Kato Y., Fiedorowicz H. *AIP Conf. Proc.*, **634** (1), 241 (2002).
9. Schulze D., Sommerer G., Drescher M., Ludwig J., Kleineberg U., Nickles P.V., Heinzmann U., Sander W. *Proc. V Int. Conf. on X-Ray Lasers* (Lund, Sweden, 1996; Bristol: IOPP, 1996) p. 353.
10. Altucci C., Bruzzese R., de Lisio C., et al. *J. Opt. A: Pure Appl. Opt.*, **2**, 289 (2000).
11. Levashov V.E., Mednikov K.N., Pirozhkov A.S., Presnyakov L.P., Ragozin E.N. *Rentgenovskaya Optika-2003* (X-ray Optics-2003) (Conference Proceedings) (N. Novgorod, 2003) p. 333.
12. Levashov V.E., Mednikov K.N., Pirozhkov A.S., Ragozin E.N. *Fiz. Plazmy*, **30** (2), 169 (2004) [*Plasma Phys. Reports*, **30** (2), 149 (2004)].
13. Malka V., Coulaud C., Geindre J.P., Lopez V., Najmudin Z., Neely D., Amiranoff F. *Rev. Sci. Instr.*, **71** (6), 2329 (2000).
14. Mori M., Shiraishi T., Takahashi E., Suzuki H., Sharmz L.B., Miura E., Kondo K. *J. Appl. Phys.*, **90** (7), 3593 (2001).
15. Dorchies F., Blasco F., Caillaud T., Stevefelt J., Stenz C., Boldarev A.S., Gasilov V.A. *Phys. Rev. A*, **68**, 023201 (2003).
16. Boldarev A.S., Gasilov V.A. *Matematicheskoe modelirovanie*, **15** (3), 55 (2003).
17. Henke B.L., Gullikson E.M., Davis J.C. *At. Data Nucl. Data Tables*, **54**, 181 (1993).
18. Soufli R., Gullikson E.M. *Proc. SPIE Int. Soc. Opt. Eng.*, **3113**, 222 (1997); http://cindy.lbl.gov/optical_constants/.
19. Andreev S.S., Zuev S.Yu., Klyuenkov E.B., Lopatin A.Ya., Luchin V.I., Salashchenko N.N., Suslov L.A. *Rentgenovskaya Optika-2003* (X-ray Optics-2003) (Conference Proceedings) (N. Novgorod, 2003) p. 226.
20. Abramovich G.N. *Prikladnaya gazovaya dinamika* (Applied Gas Dynamics) (Moscow: Nauka, 1976) p. 150.
21. Bockasten K. *J. Opt. Soc. Am.*, **51** (9), 943 (1961).